Evidence for the Modulation of *Pseudomonas aeruginosa* Exotoxin A-Induced Pore Formation by Membrane Surface Charge Density†

Dita M. Rasper and A. Rod Merrill*

Department of Chemistry and Biochemistry, Guelph–Waterloo Centre for Graduate Work in Chemistry, University of Guelph, Guelph, Ontario, Canada N1G 2W1

Received March 8, 1994; Revised Manuscript Received August 23, 1994®

ABSTRACT: The lipid requirement for the binding of wild-type *Pseudomonas aeruginosa* exotoxin A (ETA) to model endosomal membrane vesicles was evaluated using a fluorescence quenching technique. The binding of toxin to monodisperse model membrane vesicles (0.1 μm diameter) composed of various molar ratios of 1-palmitoyl-2-oleoyl-*sn*-glycero-3-phosphatidylcholine (POPC) and 1-palmitoyl-2-oleoyl-*sn*-glycero-3-phosphatidylserine (POPS) prepared by an extrusion method [Hope, M. J., *et al.* (1986) *Chem. Phys. Lipids 40* 89–107] was pH-dependent, with maximal binding observed at pH 4.0. Analysis of the binding curves indicated that the interaction of ETA with the membrane bilayer is dominated by a set of high-affinity binding sites (K_d = 2–8 μM; 60:40 (mol:mol) POPC/POPS large unilamellar vesicles (LUV)). The binding of toxin to membrane vesicles was highly pH-dependent, but was ionic strength-independent. Toxin-induced pore formation in the lipid bilayer, as measured by the release of the fluorescent dye, calcein, from LUV was pH-dependent, with optimal dye release occurring at pH 4.0. The rate of dye release from membrane vesicles decreased rapidly with increasing pH and approached zero at pH 6.0 and higher. The pK_a for this process ranged over 4.3–4.5. Calcein release from LUV was also sensitive to changes in the ionic strength of the assay buffer, with maximal release occurring at 50 mM NaCl. Higher ionic strength medium resulted in a dramatic reduction in the rate of dye release from vesicles, indicating that the toxin-induced pore is modulated by ionic interactions. Further evidence for the role of electrostatic interactions between toxin and the membrane was provided by the effect of POPS on the kinetic properties of the pore. Maximal dye release (pH 4.0) was observed for vesicles composed of 60 mol % POPS. At higher vesicle POPS content (i.e., 100 mol %), the rate of dye release was reduced by 6-fold compared with 60 mol % POPS and 2-fold compared with 20 mol % POPS. The toxin-induced membrane permeabilization was temperature-dependent, with an activation energy (E_a) near 14 kcal/mol (59 kJ/mol). A break point in the Arrhenius plot for toxin-induced pore activity indicated that the permeabilization process was sensitive to the physical state of the membrane bilayer.

Pseudomonas aeruginosa is a ubiquitous, Gram-negative bacillus that acts as an opportunistic bacterial pathogen involved in disease-inducing infections of immunocompromised patients (Vasil, 1986), such as those with cystic fibrosis or major burns. The organism produces a number of virulence factors, the most potent of which is the extracellular protein, exotoxin A (ETA[1]). ETA is believed to be largely responsible for the cytotoxic effects seen upon *Pseudomonas* bacterial infections.

Exotoxin A has been shown to exert its toxic effects by a multistep mechanism. Initially, the toxin binds to a specific eukaryotic cell surface receptor, the α_2-macroglobulin receptor (Kounnas *et al.*, 1992), and is subsequently internalized by receptor-mediated endocytosis into an endosome (Eidels *et al.*, 1983; FitzGerald *et al.*, 1980). Upon endosomal acidification, the toxin then translocates its enzymatic domain across the membrane into the cytosol (Farahbahksh & Wisnieski, 1989). Once within the cytosol, it acts to catalyze the transfer of an ADP-ribosyl moiety from NAD^+ onto elongation factor-2 (EF-2), modifying a diphthamide residue and rendering EF-2 incapable of catalyzing protein synthesis (Middlebrook & Dorland, 1984). A molecular structure consisting of three distinct domains has been assigned to ETA (Allured *et al.*, 1986), with domain I ascribed the cell binding function, domain II being responsible for membrane translocation, and domain III possessing mono-ADP-ribosyltransferase activity (Hwang *et al.*, 1987).

Membrane translocation from the lumen of the endosome to the cytoplasm of the cell is the least understood step in the toxin's mode of action. In fact, the site of toxin membrane traversal into the cytoplasm is presently controversial, since it was recently shown that ETA possesses an ER target-like sequence at its COOH terminus (Seetharam *et al.*, 1991). The stimulus for toxin translocation is believed to be acidification of the endosome (Farahbakhsh *et al.*, 1986), which leads to protein structure changes within the toxin (Farahbaksh *et al.*, 1987; Farahbakhsh & Wisnieski, 1989). One proposed mechanism for the translocation process involves an electrostatic interaction between the toxin and the inner surface of the endosomal membrane (Menestrina *et al.*, 1991).

† This research was supported by the Medical Research Council of Canada (A.R.M.).

* Author to whom correspondence should be addressed.

® Abstract published in *Advance ACS Abstracts,* October 1, 1994.

[1] Abbreviations: COOH-terminal, carboxy terminal; DMG, 3,3-dimethylglutaric acid; DPH, 1,6-diphenyl-1,3,5-hexatriene; DSC, differential scanning calorimetry; EDTA, disodium ethylenediamine tetraacetate; EF-2, elongation factor-2; ETA, exotoxin A; FBS, fetal bovine serum; FI, fluorescence intensity; IPTG, isopropyl β-D-thiogalactopyranoside; LUV, large unilamellar vesicle(s); MEM, minimal essential medium; MEMV, model endosomal membrane vesicles; PMSF, phenylmethanesulfonyl fluoride; POPC, 1-palmitoyl-2-oleoyl-*sn*-glycero-3-phosphatidylcholine; POPS, 1-palmitoyl-2-oleoyl-sn-glycero-3-phosphatidylserine; T_m, phase transition temperature; TX-100, Triton X-100; ϵ_{M280}, molar extinction coefficient (280 nm).

0006-2960/94/0433-12981$04.50/0

Within the endosome, or perhaps during the translocation event, the toxin is nicked by a protease that has not yet been identified (Ogata *et al.*, 1990). Subsequently, hydrophobic segments of the nicked toxin are exposed and inserted into the lipid bilayer, creating a pore or translocating complex that facilitates membrane traversal of the COOH-terminal half (37 kDa) of the protein. Upon exposure to the reducing environment of the cytoplasm, critical disulfide bonds are reduced, releasing the 37 kDa fragment into the cell cytosol (Ogata *et al.*, 1990). This 37 kDa catalytic fragment is capable of inactivating EF-2 and functions as a potent inhibitor of cellular protein synthesis.

In order to better characterize and understand the mechanism of the interaction of ETA with the endosomal membrane, along with subsequent toxin-induced pore formation in the membrane bilayer, a model endosomal membrane system was devised. The role of a number of factors affecting toxin binding to the membrane surface and toxin pore formation was studied, including pH, ionic strength, phosphatidylserine content, and temperature.

MATERIALS AND METHODS

Materials

The BL21(λDE3) cells were obtained from Novagen (Madison, WI); $MgSO_4$ and Triton X-100 (TX-100) were from Fisher Scientific (Nepean, ON); mouse L-M929 cells were supplied by ATCC (Rockville, MD); fetal bovine serum (FBS), minimal essential medium (MEM), and leucine-free MEM all came from Life Technologies Inc. (Grand Island, NY); isopropyl β-D-thiogalactopyranoside (IPTG) was from USB Corp. (Cleveland, OH); Q-Sepharose fast-flow anion exchange resin was obtained from Pharmacia LKB (Quebec); POPC, POPS, and 1,6-diphenyl-1,3,5-hexatriene (DPH) were all obtained from Molecular Probes Inc. (Eugene, OR); radiolabeled compounds, [^{3}H]leucine and [^{14}C]adenylate-NAD, were both supplied by DuPont-NEN Research Products (Boston, MA); polycarbonate membrane filters were purchased from Nucleopore Corp. (Pleasonton, CA). The following chemicals were obtained from Sigma Chemical Co. (St. Louis, MO): ampicillin, calcein, leucine, dimethylglutaric acid (DMG), phenylmethanesulfonyl fluoride (PMSF), Sephadex G-50, and wheat germ.

Methods

Overexpression of ETA. *Escherichia coli* strain BL21(λDE3) cells transformed with plasmid pVC45f(+)t (Chaudhary *et al.*, 1990) were grown in 50 mL of LB medium containing ampicillin (100 μg/mL) and $MgSO_4$ (10 mM) at 37 °C. When the culture reached an OD_{550} between 0.1 and 0.3, 10 mL of the culture was removed and used to inoculate each of five, 200 mL LB medium-containing flasks containing ampicillin (100 μg/mL) and $MgSO_4$ (10 mM), and the cultures were grown at 37 °C. At an OD_{550} of 0.6–0.8, the cultures were induced with 1 mM IPTG and grown for an additional 90 min at 37 °C.

Purification of Wild-Type ETA. To isolate the periplasmic fraction, 200 mL cultures (five in total) were centrifuged at 20000*g* for 10 min. Supernatants were discarded, and each pellet was resuspended in 50 mL of sucrose solution (20% sucrose, 30 mM Tris-HCl (pH 7.4), and 1 mM EDTA) and allowed to sit on ice for 10 min. The suspensions were then centrifuged at 5000*g* for 10 min. Supernatants were discarded, each pellet was osmotically shocked with 50 mL of 1 mM EDTA, 30 mM Tris-HCl (pH 7.6) solution, and the resulting suspensions were allowed to sit on ice for 10 min. The suspensions were centrifuged at 10000*g* for 10 min. All supernatants (periplasmic fraction containing ETA) were pooled and loaded onto a Q-Sepharose fast-flow anion exchange column previously equilibrated in 20 mM Tris-HCl (pH 7.6) (buffer A). After the column was washed with approximately 500 mL of buffer A, a 100 mL linear gradient of NaCl (0–1.0 M in buffer A) was developed at a flow rate of 0.5 mL/min, with the collection of 3 mL fractions. Fractions containing ETA were pooled, PMSF was added (0.01 mM final concentration), and the pool was dialyzed overnight in buffer A. The dialyzed sample was concentrated to 2.0 mL using an Amicon Centriprep concentrator (Amicon Inc., Beverly, MA). This sample was applied to a 100 × 19 mm HPLC MA7Q anion exchange column (Bio-Rad) and eluted with a linear gradient of NaCl (0–500 mM in buffer A; 3%/min, salt gradient; 3 mL/min, flow rate). The toxin eluted between 0.20 and 0.25 M NaCl. Fractions containing ETA were pooled and concentrated to 2.0 mL using an Amicon Centriprep concentrator. Protein concentration was determined by absorbance using an ϵ_{M280} of 7.85×10^4 M^{-1} cm^{-1} (O'Brien *et al.*, 1977), and purity was analyzed by SDS–PAGE (12.5% gels stained with Coomassie Brilliant Blue; Laemmli, 1970).

Cytotoxicity Assay. Samples were measured for cytotoxic activity essentially as described by Madshus and Collier (1989). Mouse L cells (L-M929) were seeded at a density of 1×10^5 cells/mL in 96-well dishes (250 μL/well), and the cells were grown in minimal essential medium (MEM) with 5% FBS for 24 h at 37 °C and 5% CO_2. At the start of the experiment, the medium was aspirated and 250 μL of fresh medium was added to each well. Toxin was added to each well (5 μL of the appropriate dilution), and the cells were incubated at 37 °C for 6 h. Medium was aspirated and replaced with leucine-free MEM containing 1 μCi of [^{3}H]-L-leucine/mL (0.25 mCi/mmol), and cells were incubated for an additional 90 min. The medium was aspirated, and cells were washed twice with 250 μL of 10% trichloroacetic acid (TCA) containing 0.1 μg of leucine/mL. Precipitated proteins were dissolved in 100 μL of 0.2 M NaOH. The contents of the microtiter plate wells were transferred quantitatively to scintillation vials and counted. Cell-associated radioactivity was determined as a measure of protein synthesis, and results are expressed as a percent of the control (no toxin added).

ADP-Ribosylation Assays. Samples were assayed for ADP-ribosylating activity, essentially as described by Kozak and Saelenger (1988). The samples were activated for 30 min at 25 °C in the presence of 4 M urea and 10 mM dithiothreitol (DTT). The samples were then incubated for 30 min at 25 °C with 0.01 μCi of [^{14}C]adenylate-NAD (1000 mCi/mmol) and wheat germ elongation factor-2 (EF-2), prepared as described by Carroll and Collier (1988), in 50 mM Tris-HCl (pH 8.2), 1 mM EDTA, and 1 mM DTT (100 μL final volume). To stop the reaction, 50 μL of each assay mixture was spotted onto 3 MM Whatman paper previously saturated with 10% TCA in ether, and then the paper was allowed to dry and ruled into individual 1 in. squares. The paper was washed twice for 30 min in 5% TCA to remove TCA-soluble material. The paper was then washed in methanol for 5 min and allowed to air-dry. The paper was cut into individual squares, and each was counted in a scintillation counter.

Preparation of LUV. Large unilamellar vesicles (LUV) were prepared by the extrusion technique of Hope *et al.* (1986). Synthetic phospholipids, POPC and POPS, in stock chloroform

solutions were mixed at various molar ratios. Lipid mixtures (1.0 mg/mL) were dried under a stream of N_2 while gently mixing and then desiccated for 1 h under vacuum. Dried lipid was resuspended in 1.0 mL of buffer containing 70 mM calcein and 50 mM NaCl (pH 7.0) by mixing under a gentle stream of N_2. The resulting large multilamellar vesicle dispersion was then transferred into an extruder device made on site. The lipid suspension was extruded through a two-stacked 25 mm polycarbonate filter with 0.1 μm pore size using nitrogen as the pressure source (100–200 psi). The extruded vesicles were collected and reinjected a total of 10 times. The LUV were applied to a Sephadex G-50 column (5 mL) and eluted with a buffer containing 160 mM NaCl, 5 mM EDTA, and 10 mM DMG (pH 4.0) (buffer B) in order to remove all external, nonencapsulated dye. Lipid concentrations were then determined using a micro Bartlett assay as previously described (Palmer & Merrill, 1993).

Dynamic Light Scattering (QELS). Vesicle size distributions were determined by QELS using a laser light source (488 nm) and instrumental setup as described previously by Strawbridge and Hallett (1992). The vesicles were prepared, the lipid concentration was adjusted to 25 μg/mL, and the sample was analyzed using the instrumentation and data analysis software reported by Hallett *et al.* (1991).

Differential Scanning Calorimetry (DSC). The phase transition temperature of the POPC/POPS bilayer was measured by high-sensitivity DSC using a Microcal MC-2D instrument at a scanning rate of 90 °C/h. Calorimetric data were filtered, converted to heat capacity, and analyzed by software provided by Microcal, Inc. Baselines were substracted from the sample thermograms.

Calcein Release Experiments. Aliquots of LUV were introduced into a fluorescence cuvette (1 cm path length) containing 2 mL of buffer B at the appropriate pH and NaCl concentration, yielding a final lipid concentration of 0.5 μg/mL. The cuvette was stirred continuously and thermostated at 23 °C, unless indicated otherwise for temperature experiments. Fluorescence intensities were measured with a Hitachi F-2000 spectrophotometer in the fluorescence ratio mode. The excitation and emission wavelengths were 494 and 520 nm (all slit widths 10 nm), respectively. Toxin-induced calcein release from vesicles was detected as an increase in fluorescence intensity due to dye dilution into the external medium (release of self-quenching dye, which occurred at calcein concentrations greater than 1 μM; data not shown). Complete (100%) dye release was detected by the addition of 0.1% Triton X-100 (final concentration). Background dye leakage from vesicles caused by changes in pH, ionic strength, etc., on LUV structural integrity (in the absence of toxin) was negligible. The rate of calcein release was determined as described in the following section.

Toxin Binding to POPC/POPS Vesicles. A fluorescence binding assay was devised to measure the dissociation constants for toxin–vesicle interactions. Unilamellar vesicles (0.1 μm av diam) were prepared by mixing various amounts of POPC and POPS. To each liposome preparation was added 5% DPH-PC (wt probe: total wt lipid), and the vesicles were prepared as described earlier except that no calcein was entrapped in the liposomes. A solution of toxin (5 μg/mL) in 10 mM DMG and 100 mM NaCl (adjusted to the appropriate pH with NaOH) was titrated with lipid by successive additions to a thermostated and stirred quartz cuvette. Toxin intrinsic fluorescence emission (Trp and Tyr) was measured in a PTI Alphascan-2 spectrofluorimeter with λ_{ex} = 280 nm and λ_{em} scanned from 300 to 420 nm (excitation and emission slits 5 and 10 nm, respectively). A blank (no toxin) for each lipid concentration in the corresponding buffer was subtracted from each sample (containing toxin and lipid). The corrected fluorescence emission spectra were used to determine the extent of quenching caused by DPH-PC on the intrinsic toxin fluorescence.

Analysis of Binding Data. Binding data were analyzed according to conventional binding theory (Wyman & Gill, 1990):

$$T + nL \rightleftharpoons TL_n \quad (1)$$

where one molecule of toxin (T) forms a complex (TL_n) with n molecules of lipid (Surewicz & Epand, 1984; Jain *et al.*, 1985). For the situation where the interaction of toxin with the lipid substrate is non-cooperative and does not affect the interaction of additional peptide with the same vesicle, or in the case of independent binding sites, the following binding isotherm may be applied:

$$X = [T_f]/(K_d + n[T_f]) \quad (2)$$

Then X is the number of moles of toxin bound (T_b) per mole of total lipid (L_T), $[T_f]$ is the free toxin concentration, and K_d is the dissociation constant.

From the fluorescence measurements, the values of $[T_b]$ and the parameter X may be determined. The value of $[T_b]$ associated with the lipid phase is given by

$$[T_b] = [T_T](F - F_o)/(F_{max} - F_o) \quad (3)$$

where $[T_T]$ is the total toxin concentration, F_o is the intrinsic toxin fluorescence in the absence of lipid, F_{max} is the plateau value of the fluorescence intensity obtained from a measurement where a very large excess of lipid vesicles was added to the toxin, and F is the fluorescence intensity after each successive addition of lipid. The data were analyzed by a nonlinear curve-fitting program, Origin (Microcal Inc., CA), where the preceding algorithms were used to fit the fluorescence titration data.

Kinetic Analysis of Toxin-Induced Dye Efflux from LUV. The kinetic analysis of toxin-induced pore formation in membranes was treated according to Schwartz and Robert (1990). The fluorescence signal obtained during the toxin-induced efflux of calcein from LUV was used in a normalized efflux function,

$$E(t) = (F_\infty - F)/(F_\infty - F_o) \quad (4)$$

which describes the measured release of calcein as a function of time. Here, F_∞ is the fluorescence intensity upon total release (lysis) of the vesicles with Triton X-100, F is the fluorescence intensity for the efflux at each time point (1 s intervals), and F_o is the fluorescence intensity at zero time. The data were analyzed and fit using a computer program designed solely for that purpose. The vesicles, after extrusion, were analyzed for their size distribution by QELS (Hallet *et al.*, 1991) and found to be quite homogeneous (diameter, 120 ± 21 nm; see preceding sections). This vesicle size homogeneity simplifies the kinetic analysis of dye release from these liposomes. The number of vesicles per milliliter was determined as

$$N = n_L N_A/\nu \quad (5)$$

where N is the total number of liposomes in the system, n_L

is the number of moles of lipid in all vesicles, N_A is Avogadro's number, and ν is the number of lipid molecules/single liposome.

Calcein Efflux through a Single Pore. According to Fick's first law,

$$-(dn/dt) = A_p D_o (c - c')/d \quad (6)$$

where n is the amount of dye (moles) at time t inside a vesicle, c and c' are the internal and external dye concentrations, respectively, A_p is the effective cross section of the pore, D_o is the diffusion coefficient of marker molecules in the pore, and d is the pore length (i.e., the thickness of the membrane). It is assumed that the intravesicular concentration equilibrates sufficiently fast, so that $n = (4\pi/3)R^3c$ and c' can be taken as a constant. Given these conditions, eq 3 can be solved, resulting in

$$c - c' = (c_o - c') \exp^{-t/\tau_o} \quad (7)$$

(c_o is the given value of c_o at $t = 0$), reflecting the intrinsic release time,

$$\tau_o = (4\pi/3)R^3 d/A_p D_o \quad (8)$$

where τ_o is the relaxation time and R is the vesicle radius.

For an ETA-induced pore, where the bilayer thickness is 40 Å, the S_R of calcein is 0.5 nm, the vesicle diameter is 0.1 μm, and the relaxation time (τ_o) is 2.6×10^{-2} s. The concentration gradient in the vesicles will be established very much faster ($d^2/2D_o \approx 10^{-8}$ s), and the time for reequilibrating any change in internal calcein concentration is also more rapid ($R^2/6D_o \approx 10^{-7}$s) than the relaxation time (Schwarz & Robert, 1990).

The normalized efflux function ($E(t)$) with respect to the rate of pore formation can be expressed as

$$E(t) = e^{-p(t)} \quad (9)$$

where $p(t)$ is the average number of pores per vesicle. Then the velocity of pore formation can be described by

$$v_p = (dr_p/dt)_{forward} \quad (10)$$

with v_p being the forward rate of pore formation, and $r_p = n_p/n_L$ (the molar ratio of pores/lipid). Integration of eq 10 and division by N gives

$$p(t) = v \int v_p dt$$

According to Schwartz and Robert (1990), the pore number function can be readily determined from the experimental efflux function. Recall eq 9, $E(t) = e^{-p(t)}$, then $-\ln E(t) = p(t)$, and a plot of $-\ln E(t)$ against t should give a slope of $p = dp/dt = v/v_p$ = no. of lipid molecules/cell × no. of pores/lipid·second = no. of pores/cell·second. The initial slope then defines a first-order rate constant related to single vesicles of uniform size:

$$k_o = (dp/dt)_{t=0} = vv_p \quad (11)$$

RESULTS

Toxin Binding to Membrane Vesicles

Effect of Phosphatidylserine Content (POPS). Figure 1 shows that the binding of ETA (pH 4.0) to model endosomal membrane vesicles (MEMV) is modulated by the amount of POPS present in the membrane. The various binding curves

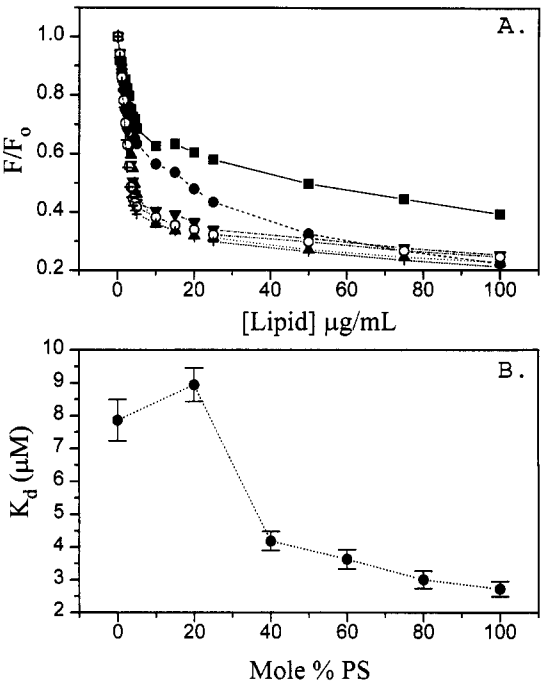

FIGURE 1: (A) Effect of POPC/POPS lipid composition on ETA binding to LUV at pH 4. The intrinsic fluorescence of ETA was measured with λ_{ex}, 280 nm, and λ_{em}, 333 nm (excitation and emission bandpasses were 2 and 4 nm, respectively): temperature, 20 °C; 10 mM DMG buffer and 100 mM NaCl, pH 4; LUV were prepared by extrusion through 0.1 μm polycarbonate membranes. Each vesicle/phospholipid mixture contained 5% DPH-PC (Molecular Probes, Inc.). The POPC:POPS (mol:mol) ratios were (■) 100:0, (●) 80:20, (▲) 60:40, (▼) 40:60, (○) 20:80, and (+) 0:100. Protein concentrations were 5 μg/mL. (B) Effect of POPC/POPS lipid composition on the dissociation constants for ETA binding to LUV at pH 4. The dissociation constants (K_d, μM) for the ETA–membrane interactions were calculated from the data presented in A.

for ETA and MEMV composed of varying amounts of POPS are shown in Figure 1A. The binding data were analyzed according to standard macromolecular binding theory (Wyman & Gill, 1990; see Materials and Methods). The dissociation constants (apparent K_d values) for the ETA–membrane interaction were calculated from the data presented in Figure 1A and are shown in Figure 1B. The strength of the interaction varied from a dissociation constant of 8 μM for 100% POPC vesicles to 2.5 μM at 100% POPS (Figure 1B). Toxin binding to the membrane remained relatively constant at 40 mol % POPS or higher.

Effect of pH on ETA Binding. Since the extent of toxin binding to the membrane surface did not change significantly at compositions greater than 40% POPS, a single lipid composition (60 mol % POPS) was chosen for further study (Figure 1A,B). The effect of pH on toxin binding to 60 mol % POPS vesicles is shown in Figure 2A,B. The strength of the macromolecular association between toxin and vesicles was highly pH-dependent, with maximal binding occurring at pH 4.0 and minimal binding at pH 7.0. The dissociation constant was 40-fold higher at pH 7.0 compared with pH 4.0 and showed a 5-fold increase between pH 6.0 and 7.0 (Figure 2B).

Effect of Ionic Strength on ETA Binding. The association of toxin with the membrane surface was sensitive to the ionic strength of the bulk medium (Figure 3A). More toxin was bound to the vesicles at 0.1 M NaCl, with a significant decrease in the extent of bound toxin seen upon raising the ionic strength from 0.1 to 0.5 M. Further increases in the ionic strength (0.7 and 0.9 M NaCl) resulted in little or no change in the

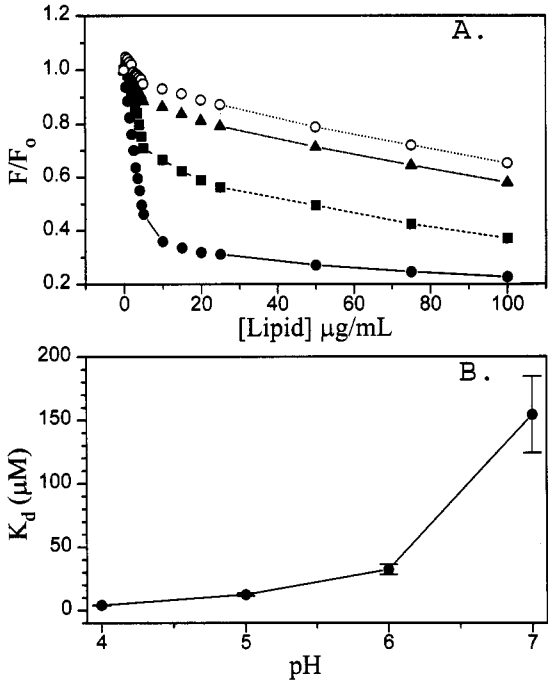

FIGURE 2: (A) Effect of pH on ETA binding to POPC/POPS (60:40, mol:mol) LUV. Conditions as per Figure 1A. The various pH solutions were (●) pH 4, (■) pH 5, (▲) pH 6, and (○) pH 7. (B) Effect of pH on the dissociation constants for ETA binding to POPC/POPS (60:40, mol:mol) LUV. The dissociation constants (K_d, μM) for the ETA–membrane interactions were calculated from the data presented in A.

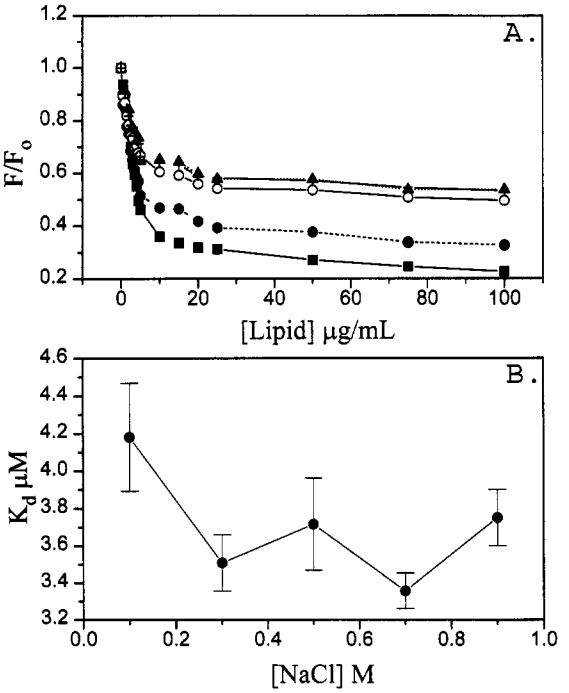

FIGURE 3: (A) Effect of ionic strength on ETA binding to POPC/POPS (60:40, mol:mol) LUV at pH 4. Conditions were as per Figure 1A. NaCl concentrations were (■) 0.1 M, (●) 0.3 M, (▲) 0.5 M, (○) 0.7 M, and (+) 0.9 M. (B) Effect of ionic strength on the dissociation constants for ETA binding to POPC/POPS (60:40, mol:mol) LUV. The dissociation constants (K_d, μM) for ETA–membrane interactions were calculated from the data presented in A.

amount of toxin bound to the vesicles (Figure 3A). While the extent of toxin binding is dependent upon ionic strength, the magnitude of the association between toxin and vesicle is not affected by the ionic strength of the binding medium (Figure 3B). Thus, as the concentration of NaCl in the medium

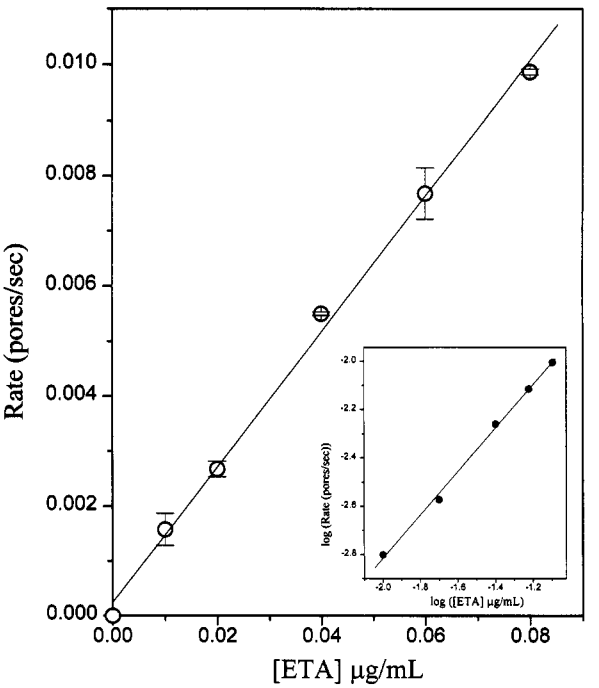

FIGURE 4: Effect of ETA concentration on the rate of pore formation for POPC/POPS (40:60, mol:mol) LUV at pH 4 and 160 mM NaCl. Pore formation was monitored by the release of vesicle-entrapped calcein. Calcein fluorescence was measured with λ_{ex} = 494 nm (slit width, 5 nm) and λ_{em} = 520 nm (slit width, 10 nm): buffer, 160 mM NaCl, 5 mM EDTA, and 10 mM DMG, pH 4; temp, 23 °C. One hundred percent calcein release was determined by the addition of 0.1% TX-100 (final concentration). The rate of pore formation was calculated as described in Materials and Methods. The POPC/POPS vesicle composition used was 40:60 (mol:mol). Inset: Plot of log rate against log toxin concentration.

increased, the number of binding sites for the toxin decreased. The effect of varying the solution ionic strength on the toxin's aromatic fluorescence was measured (data not shown), with results similar to those obtained previously by Jiang and London (1990). Variation in the solution ionic strength caused no significant conformational change in the toxin.

Toxin-Induced Pore Formation

Effect of ETA Concentration on Calcein Release. Figure 4 shows the dependence of calcein release from LUV on ETA concentration for 60 mol % POPS vesicles at pH 4.0. Toxin-induced pore formation, as measured by the rate of calcein release from vesicles (pH 4, 160 mM NaCl), saturated at an ETA concentration of 0.1 μg/mL for all vesicle compositions except the 80:20 (mol:mol) vesicles, which saturate at 0.05 μg/mL toxin (data not shown). The rate of dye release from vesicles under optimal conditions (pH 4.0, 60% POPS or higher) indicated that there was a first-order dependence with respect to toxin concentration. A plot of log rate against log toxin concentration (Figure 4, inset) was also linear with a slope of 0.9, indicating that a single toxin entity is responsible for the formation of the pore in the liposome bilayer. This may be a monomeric toxin species (single molecule) or perhaps an oligomeric structure; the latter possibility must include a preformed aggregate that contacts the membrane surface. These data exclude the possibility of oligomerization occurring subsequent to the binding of toxin to the vesicle surface (Shiver & Donovan, 1987).

Effect of pH on Calcein Release. Toxin-induced pore formation was shown to be pH-dependent (Figure 5), reaching a maximum near pH 4 for all liposome compositions. At pH 4.0, a progressive decrease in the rate of dye release (pore

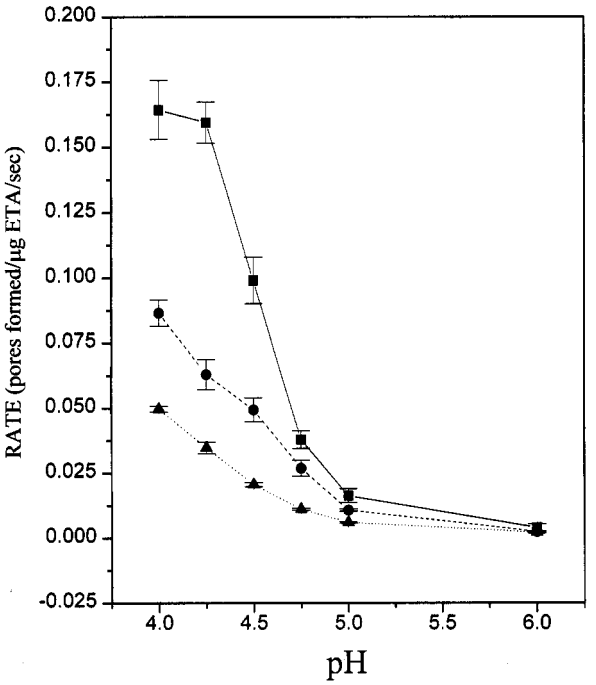

FIGURE 5: Effect of pH on the rate of pore formation for various POPC/POPS (mol:mol) LUV. The buffer consisted of 160 mM NaCl, 5 mM EDTA, and 10 mM DMG, with varying pH values. Final lipid concentration was 5 μg/mL. Protein concentrations ranged from 0.005 to 0.1 μg/mL, depending on the response elicited. Remaining conditions were as per Figure 4. The POPC POPS (mol:mol) ratios were (■) 0:100, (●) 40:60, and (▲) 80:20.

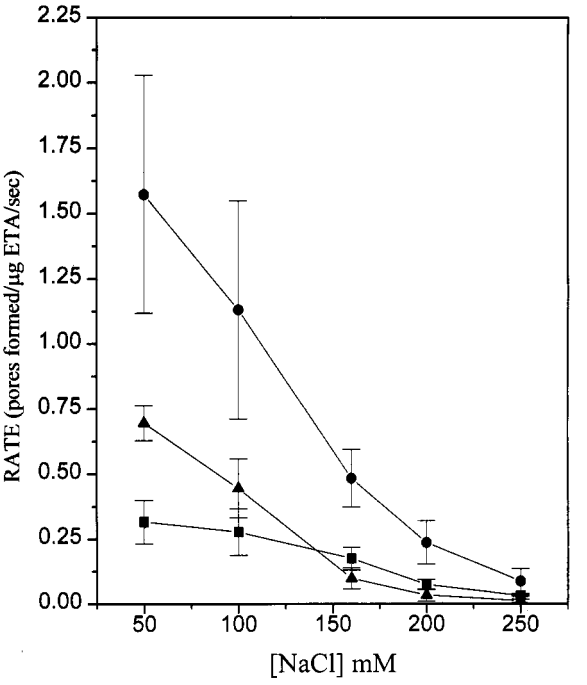

FIGURE 6: Effect of ionic strength on the rate of pore formation for various POPC/POPS (mol:mol) LUV. The buffer consisted of 5 mM EDTA and 10 mM DMG (pH 4) with varying concentrations of NaCl (0–300 mM). Final lipid concentration was 5 μg/mL. Protein concentrations ranged from 0.005 to 0.1 μg/mL, depending on the response elicited. Remaining conditions were as per Figure 4. The POPC:POPS (mol:mol) ratios were (■) 0:100, (●) 40:60, and (▲) 80:20.

formation) was observed as the amount of POPS in the vesicle preparation decreased. The rate of dye release approached zero at pH values higher than 5.0. The curvilinear nature of the data indicated the involvement of more than one event in the mechanism of pore formation by ETA.

Table 1 indicates the effect of varying the POPC:POPS ratio on the pK_a of the toxin-induced dye release event. The pK_a ranged from 4.3 to 4.5, with no significant differences existing between the various vesicle compositions.

Effect of Ionic Strength on Calcein Release. All vesicle compositions demonstrated similar trends with respect to the shape of the curves for calcein release as a function of the ionic strength of the solution (Figure 6). The maximal rate of dye release was observed at 50 mM NaCl for all vesicle compositions. At higher ionic strengths (50–150 mM), there was a sharply progressive decrease in the amount of dye released per microgram of ETA. At NaCl concentrations of 200 mM or higher, the rate of dye release for all vesicle compositions became negligible. Furthermore, the magnitude of dye release and, hence, the rate of pore formation were the lowest for vesicles composed of 100 mol % POPS. Maximal rates were observed for vesicles with 60 mol % POPS and intermediate rates for those vesicles composed of 20 mol % POPS. In the case of 0 mol % POPS (100 mol % POPC) vesicles, the rate was not detectable under these conditions because copious amounts of toxin were required to elicit detectable dye release from liposomes.

Effect of Temperature on Rate of Calcein Release. The effect of temperature on toxin-mediated dye release from vesicles is shown in Figure 7. This Arrhenius plot depicts the natural logarithm of the first-order rate constant for toxin-induced calcein release from LUV plotted against the inverse temperature (degrees Kelvin) at pH 4.0 for vesicles consisting of 60 mol % POPS. A break point in the plot was seen corresponding to a temperature of 15 °C. The phase transition

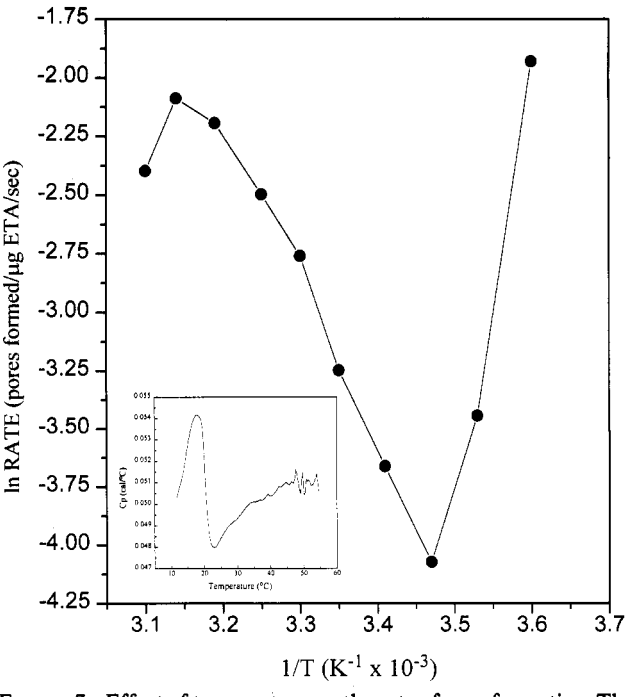

FIGURE 7: Effect of temperature on the rate of pore formation. The POPC/POPS vesicle composition used was 40:60 (mol:mol). Final lipid concentration was 5 μg/mL. Protein concentrations ranged from 0.005 to 0.1 μg/mL, depending on the response elicited. Remaining conditions were as per Figure 4. Parameters for anisotropy measurements were as described in Materials and Methods. Inset: Differential scanning calorimetry thermogram for POPC/POPS bilayers (40:60, mol:mol); see Materials and Methods for details.

temperature (T_m) measured by DSC (differential scanning calorimetry) for POPC/POPS vesicles, although somewhat broad, is centered near 18 °C (Figure 7, inset). This value is higher than the previously reported value for POPC vesicles

(T_m = −2 °C) as measured by differential scanning calorimetry (DSC; Small, 1986). However, the presence of a mixture of POPC/POPS may account for the relatively high T_m's of these membrane bilayers since PS bilayers generally cause a shift to higher T_m values as compared with PC bilayers (Marsh, 1990). The pronounced break point observed in the Arrhenius plot indicated that the process of pore formation in the membrane by ETA may be sensitive to the physical state of the membrane bilayer. However, the effect is masked by the observed increase in membrane vesicle leakiness at temperatures at or below the T_m for the phospholipid. At temperatures below the T_m, the rate of vesicle dye release increased dramatically, rather than plateauing at a near-zero level. Also, at higher temperature (45–50 °C), the toxin-induced pore appeared to undergo inactivation (Figure 7). The energy of activation (E_a) for toxin-induced dye release from POPC/POPS (40:60 mol %) vesicles, as calculated from the slope of the line extending from 15 to 40 °C, is 14 kcal/mol (59 kJ/mol).

DISCUSSION

The binding of ETA to the membrane bilayer is influenced by the net charge at the membrane surface (Figure 1B). An increase in the negative charge density at the surface of the membrane leads to tighter binding of the toxin. However, a threshold concentration of negative charges exists above which there is no further increase in the strength of membrane binding by the toxin. The increased binding of toxin in the presence of negatively charged phospholipids is most likely due to a reduced local pH in the proximity of the vesicle surface (Menestrina *et al.*, 1989).

The effect of pH on toxin function has been described previously (Menestrina *et al.*, 1991), and our results are in agreement with those reported by Menestrina *et al.*; however, Menestrina and co-workers made no attempt to calculate a dissociation constant for the toxin–vesicle interaction. Despite the fact that these calculated dissociation constants are only apparent binding constants (Kuchinka & Seelig, 1989), they serve as useful relative measures of binding affinity between the toxin and various MEMV. The binding of toxin to the membrane was high-affinity at pH 4.0 (K_d = 3.3 μM), with a 6-fold reduction in affinity at pH 6 followed by a 30-fold reduction in affinity at pH 7.0. This association of toxin with MEMV was optimal near the pH 4–5 range, which corresponds to the pH of the endosomal vesicle within the cell (Helenius *et al.*, 1983).

The enhanced avidity of toxin binding to membrane vesicles observed with decreasing pH can be correlated with a pH-induced conformational change in the toxin. This change resulted in a 3-fold enhancement in the FI of ETA, but no significant change in the fluorescence $\lambda_{em\ max}$ (data not shown). These results correlate with the enhanced exposure of at least some aromatic residues of the toxin upon acidification of the external solution medium, suggesting a low-pH-induced conformational change in the toxin, which corroborates previous results reported by Jiang and London (1990).

The effect of ionic strength on the association of toxin with the vesicle surface was surprising. There was no apparent difference in the K_d values for toxin binding from 0.1 to 0.9 M NaCl (Figure 3B). This difference indicated that the number of toxin binding sites decreased as the ionic strength increased (Figure 3A). Therefore, the interaction of toxin with model membrane vesicles is at least partially electrostatic in nature. It is possible that the initial interaction between ETA and the vesicle surface involves an electrostatic association with the phospholipid headgroup, which may then lead to hydrophobic contact between the toxin and the hydrocarbon core of the bilayer.

Table 1: Effect of pH on the pK_a of Pore Formation for Various POPC/POPS (mol:mol) LUV

POPC/POPS (mol:mol)	pK_a[b]	SD[a]
0:100	4.48	0.59
40:60	4.42	0.51
80:20	4.32	0.38

[a] Errors are the standard deviation from three or more experiments. [b] The pK_a values were determined from the rate data presented in Figure 5. Rate curves were fit by a least-squared linear regression analysis. The fit rate data were converted to natural logarithm values and plotted as a function of solution pH. Maximum and minimum rate values were then fit to the equation of the line to interpolate the pK_a value for each different vesicle composition study.

Furthermore, the fluorescence results (data not shown) indicate that there is no significant structural change in ETA induced by varying the ionic strength of the solution, which agrees with previous results (Jiang & London, 1990). This result indicated that the ionic strength effect on the toxin-induced pore-forming activity is likely due to ionic screening of electrostatic groups on the surface of both the protein and the membrane and probably is not a result of protein structural change.

The formation of a pore by ETA follows first-order kinetics with respect to toxin concentration (Figure 4). These data suggest a single-hit mechanism for toxin-induced membrane leakage, as seen for the pore-forming colicins E1 and Ia (Peterson & Cramer, 1987; Mel & Stroud, 1993) and for diphtheria toxin (Shiver & Donovan, 1987). Two explanations are possible for this observed mechanism: (i) a single molecule of toxin forms a pore in the membrane bilayer or (ii) a preformed oligomeric species contacts the membrane surface to form a pore. The stoichiometry of toxin per vesicle was calculated at 100:1 (toxin:vesicle, 0.01 μg of toxin and 0.5 μg of phospholipid). This translates into a phospholipid:toxin ratio of 5000. The concentration of toxin required to release 100% of the calcein from the vesicles was 0.1 μg/mL at 0.5 μg/mL phospholipid (data not shown). This indicated that, at maximal dye release, 1000 molecules of toxin were present in solution per phospholipid vesicle. Clearly, these data imply that not all toxin molecules are functional. If a monomeric toxin species forms a functional pore, then 0.1% of the toxin molecules form an active pore in POPC/POPS (40:60 mol:mol) vesicles.

Toxin-induced dye release from vesicles reached a maximum at pH 4.0 (Figure 5) and decreased at lower pH values (data not shown). This phenomenon exhibited a pK_a between 4.3 and 4.5 for the various POPC/POPS liposomes (Table 1), which is in general agreement with previous results (Menestrina *et al.*, 1991; pK_a = 4.5). This indicates that the likely candidates for ionizable groups within the toxin molecule responsible for pore formation are Asp and Glu residues, which upon protonation may facilitate toxin binding to the negatively charged membrane surface, i.e., perhaps due to protein amino groups associating with carboxylate groups within the POPS headgroup being facilitated by the reduction in charge repulsion from Asp/Glu side chain carboxylate groups.

The kinetics of pore formation by toxin was dependent upon the ionic strength of the medium (Figure 6), with the rate of dye release maximal at 50 mM NaCl. However, an unexpected result was seen when the effect of ionic strength on the rate of toxin-induced pore formation was correlated with the POPS

vesicle content. At low ionic strength (50 mM), vesicles composed of lower amounts of POPS (40 mol %) were far better substrates for toxin pore-forming activity compared to vesicles prepared with higher concentrations of POPS (100 mol % POPS). If the POPS content was lowered even further (20 mol %), however, rates were observed to be intermediate. Higher ionic strength values (ca. 150 mM NaCl) resulted in a much smaller difference between the rates of pore formation for the various liposome compositions (Figure 6). These results imply that there is an optimal POPS vesicle composition for pore formation and indicate that there is an optimal negative charge density at the vesicle membrane surface required for toxin-induced vesicle permeabilization. If the charge density is too sparse (20 mol % POPS), then the toxin cannot form a functional pore due to insufficient association energy; if the density is too high (100 mol % POPS), then perhaps the toxin is locked in a conformation at the membrane surface that is nonfunctional. An optimal density of negative charge is needed to hold the toxin sufficiently strongly to the membrane surface but not so tightly as to inhibit the conformational rearrangement of the toxin required for the insertion event, which leads to a functional pore being formed within the vesicle bilayer. However, one caveat to these studies is that the effects of osmolarity (vesicle tonicity) and membrane potential were not studied and these parameters may also modulate the action of *Pseudomonas* exotoxin A on membranes.

The toxin-induced pore was sensitive to the physical state of the membrane bilayer (Figure 7) and was modulated by membrane microviscosity. This was inferred from the break point observed in the Arrhenius plot for toxin pore kinetics near 15 °C, since this temperature corresponds with the measured T_m for POPC/POPS vesicles (Figure 7, inset). However, it appeared that the membrane bilayer became more fragile at temperatures below the T_m because instead of leveling off, the rate of dye release increased dramatically as the temperature (below the T_m) was decreased. The calculated activation energy (E_a) for the toxin-induced pore formation event (above the T_m) was 13.73 kcal/mol (57.4 kJ/mol). This activation energy barrier for toxin and vesicle interaction is similar to the value reported by Menestrina *et al.* (1989) for tetanus toxin and PC/PS vesicles at pH 4.0.

The following mechanism is proposed for ETA binding, insertion, and subsequent pore formation in MEMV:

$$ETA_f \underset{k_{-b}}{\overset{k_b}{\rightleftharpoons}} ETA_b \xrightarrow{k_p} ETA_p$$

where ETA_f is the free toxin, ETA_b is the membrane-bound toxin, ETA_p is the toxin pore existing in the membrane, k_b and k_{-b} are the toxin on and off rates, respectively, and k_p is the rate constant for pore formation by toxin. The transition from ETA_b to ETA_p is modulated, at least in part, by the density of negative charge near the phospholipid headgroup of the MEMV surface. A model, albeit highly speculative at this stage, can be envisioned for the permeabilization of the membrane bilayer by ETA, which is a direct result of the translocation process for the toxin (Figure 8). The first step in the mechanism is the binding of the toxin to the membrane surface induced by acidification of the medium. This has both an electrostatic and a hydrophobic component. The second step in the mechanism is the insertion of the toxin into the membrane bilayer, which is modulated by the local charge at the membrane surface. Insertion of part or all of domain II and possibly other regions of the toxin molecule leads to permeabilization of the membrane. The translocation of domain III across the membrane is then initiated, ultimately leading to the complete translocation of domain III to the other side of the membrane.

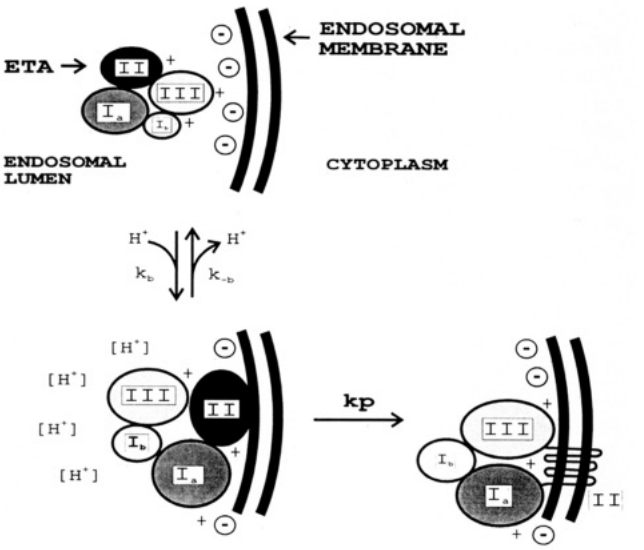

FIGURE 8: Model for ETA binding and permeabilization. A schematic diagram of the interaction of ETA with the endosomal membrane based on the results presented in this paper. The specific membrane-associated topology of the toxin has not been elucidated and is only inferred from this study and other previous studies.

ACKNOWLEDGMENT

We thank Dr. David FitzGerald for kindly providing plasmid pVC45f(+)T for exotoxin A production. We also acknowledge the invaluable contribution of Dr. Uwe Oehler for writing the computer program for the analysis of the kinetic data.

REFERENCES

Allured, V. S., Collier, R. J., Carroll, S. F., & McKay, D. B. (1986) *Proc. Natl. Acad. Sci. U.S.A.* 83, 1320–1324.
Carroll, S. F., & Collier, R. J. (1988) *Methods Enzymol. 165*, 218–225.
Chaudhary, V. K., Jinno, Y., Gallo, M. G., FitzGerald, D., & Pastan, I. (1990) *J. Biol. Chem. 265*, 16306–16310.
Eidels, L., Proia, R. L., & Hart, D. A. (1983) *Microbiol. Rev. 47*, 596–620.
Farahbakhsh, Z. T., & Wisnieski, B. J. (1989) *Biochemistry 28*, 580–585.
Farahbakhsh, Z. T., Baldwin, R. L., & Wisnieski, B. J. (1986) *J. Biol. Chem. 261*, 11404–11408.
Farahbakhsh, Z. T., Baldwin, R. L., & Wisnieski, B. J. (1987) *J. Biol. Chem. 262*, 2256–2261.
FitzGerald, D., Morris, R. E., & Saelinger, C. B. (1980) *Cell 21*, 867–873.
Hallett, F. R., Watton, J., & Krygsman, P. (1991) *Biophys. J. 59*, 357–362.
Helenius, A., Mellman, I., Wall, D., & Hubbard, A. (1983) *Trends Biochem. Sci. 8*, 245–254.
Hope, M. J., Bally, M. B., Mayer, L. D., Janoff, A. S., & Cullis, P. R. (1986) *Chem. Phys. Lipids 40*, 89–107.
Hwang, J., FitzGerald, D. J., Adhya, S., & Pastan, I. (1987) *Cell 48*, 129–136.
Jain, M. K., Rogers, J., Simpson, L., & Gierasch, L. (1985) *Biochim. Biophys. Acta 816*, 153–162.
Jiang, J. X., & London, E. (1990) *J. Biol. Chem. 265*, 8636–8641.
Kounnas, M. Z., Morris, R. E., Thompson, M. R., FitzGerald, D. J., Strickland, D. K., & Saelinger, C. B. (1992) *J. Biol. Chem. 267*, 12420–12423.
Kozak, K. J., & Saelinger, C. B. (1988) *Methods Enzymol. 165*, 147–152.

Kuchinka, E., & Seelig, J. (1989) *Biochemistry 28*, 4216–4221.
Laemmli, U. K. (1970) *Nature (London) 227*, 680–685.
Madshus, I. H., & Collier, R. J. (1989) *Infect. Immun. 57*, 1873–1878.
Marsh, D. (1990) in *Handbook of Lipid Bilayers*, CRC Press, Boston.
Mel, S. F., & Stroud, R. M. (1993) *Biochemistry 32*, 2082–2089.
Menestrina, G., Forti, S., & Gambale, F. (1989) *Biophys. J. 55*, 393–405.
Menestrina, G., Pederzolli, C., Forti, S., & Gambale, F. (1991) *Biophys. J. 60*, 1388–1400.
Middlebrook, J. L., & Dorland, R. B. (1984) *Microbiol. Rev. 48*, 199–221.
O'Brien, A. D., Thompson, M. R., Geriski, P., Doctor, B. P., & Formal, S. B. (1977) *Infect. Immun. 15*, 796–801.
Ogata, M., Chaudhary, V. K., Pastan, I., & FitzGerald, D. J. (1990) *J. Biol. Chem. 265*, 20678–20685.
Palmer, L. R., & Merrill, A. R. (1994) *J. Biol. Chem. 269*, 4187–4193.
Peterson, A. A., & Cramer, W. A. (1987) *J. Membr. Biol. 99*, 197–204.
Schwartz, G., & Robert, C. H. (1990) *Biophys. J. 58*, 577–583.
Schwartz, G., & Robert, C. H. (1992) *Biophys. Chem. 301*, 4622–4627.
Seetharam, S., Chaudhary, V. K., FitzGerald, D. J., Pastan, I. (1991) *J. Biol. Chem. 266*, 17376–17381.
Shiver, J. W., & Donovan, J. J. (1987) *Biochim. Biophys. Acta 903*, 48–55.
Small, D. M. (1986) in *Handbook of Lipid Research*, Vol. 4, *The physical chemistry of lipids: from alkanes to phospholipids* (Small, D. M., Ed.) pp 598–635, Plenum Press, NY.
Strawbridge, K. B., & Hallett, F. R. (1992) *Can. J. Phys. 70*, 401–406.
Surewicz, W. K., & Epand, R. M. (1984) *Biochemistry 23*, 6072–6077.
Vasil, M. L., Chamberlain, C., & Grant, C. R. C. (1986) *Infect. Immun. 52*, 538–548.
Wyman, J., & Gill, S. J. (1990) in *Binding and Linkage*, Chapter 1, pp 1–31, University Science Books, Mill Valley, CA.